CHEMISTRY OF MATERIALS
Article

Chem. Mater. **2009,** *21,* 4305–4309 4305
DOI:10.1021/cm901615n

Synthesis of ZnSe/CdS/ZnSe Nanobarbells Showing Photoinduced Charge Separation

Maria Kirsanova, Alexander Nemchinov, Nishshanka N. Hewa-Kasakarage, Nicholas Schmall, and Mikhail Zamkov*

The Center for Photochemical Sciences and Department of Physics, Bowling Green State University, Bowling Green, Ohio 43403

Received June 11, 2009. Revised Manuscript Received July 29, 2009

We report on a colloidal synthesis of barbell-shaped nanocrystals comprising a type II heterojunction of ZnSe and CdS domains and showing compelling evidence of photoinduced charge separation at the interface of ZnSe and CdS materials. The nanobarbells were fabricated in a two-step procedure by growing ZnSe caps onto polar facets of CdS nanorods. Under present synthetic conditions, minimal growth of ZnSe shell in the lateral direction and focusing of the barbell length distribution were observed. Formation of epitaxial interfaces between nearly lattice-matched ZnSe and CdS crystal phases was primarily evidenced by the observation of "spatially indirect" fluorescence and long radiative lifetimes corresponding to the decay of charge transfer states.

1. Introduction

Colloidal semiconductor nanocrystals (NCs) are emerging as promising building blocks for the development of the new generation of low-cost optoelectronic materials with potential applications in solar cells,[1] lasers,[2] biomedical labels,[3] and light-emitting diodes.[4] The ability to incorporate a desired combination of properties within these nanostructures often depends on the existence of synthetic protocols for conjoining of two or more semiconductor materials into composite nanoscale objects. To achieve this goal, synthetic efforts in this area have been focused on the development of multifunctional heterostructures with architectures that range from symmetric core/shell geometries[5−14] to more complex shapes including dot-in-a-rod,[15−17] barbells,[18,19] heterodimers,[20,21] tetrapods,[22] and multibranched structures.[23]

Recently, heterostructured NCs exhibiting photoinduced charge separation have become the subject of an increasing number of investigations due to their potential use in photovoltaic and photocatalytic applications. Spatial separation of electrons and holes in these materials is achieved via a staggered alignment of band edges at the boundary of nanocrystalline domains that form the composite nano-object. Several combinations of semiconductors, including CdTe/CdSe,[9,10,24] ZnTe/CdS,[25] and ZnSe/CdS,[7,8] assembled either by nucleating the growth of spherical caps on polar facets of nanorods (NRs) or by growing two or more linear extensions at high-energy surfaces of seeding nanocrystals, have been explored for the development of type II heterojunctions showing long-lived charge separated states. To date, most favorable characteristics both in terms of the spatial separation as

*Corresponding author. E-mail: zamkovm@bgsu.edu.

(1) Kamat, P. V. *J. Phys. Chem. C* **2008**, *112*, 18737.
(2) Klimov, V. I.; Mikhailovsky, A. A.; Xu, S.; Malko, A.; Hollingsworth, J. A.; Laetherdale, C. A.; Eisler, H. J.; Bawendi, M. G. *Science* **2000**, *290*, 314.
(3) Medintz, I. L.; Uyeda, H. T.; Goldman, E. R.; Mattoussi, H. *Nat. Mat.* **2005**, *4*, 435.
(4) Coe, S.; Woo, W. K.; Bawendi, M.; Bulovic, V. *Nature* **2002**, *420*, 800.
(5) Kim, S.; Fisher, B.; Eisler, H. J.; Bawendi, M. *J. Am. Chem. Soc.* **2003**, *125*, 11466.
(6) Schöps, O.; Thomas, N. L.; Woggon, U.; Artemyev, M. V. *J. Phys. Chem. B* **2006**, *110*, 2074.
(7) Yu, K.; Zaman, B.; Romanova, S.; Wang, D.; Ripmeester, J. *Small* **2005**, *1*, 332.
(8) Xie, R.; Zhong, X.; Basché, T. *Adv. Mater.* **2005**, *17*, 2741.
(9) Cheng, C. T.; Chen, C. Y.; Lai, C. W.; Liu, W. H.; Pu, S. C.; Chou, P. T.; Chou, Y. H.; Chiu, H. T. *J. Mater. Chem.* **2005**, *15*, 3409.
(10) Danek, M.; Jensen, K. F.; Murray, C. B.; Bawendi, M. G. *Chem. Mater.* **1996**, *8*, 173.
(11) Ivanov, S. A.; Nanda, J.; Piryatinski, A.; Achermann, M.; Balet, L. P.; Bezel, I. V.; Anikeeva, P. O.; Tretiak, S.; Klimov, V. I. *J. Phys. Chem. B* **2004**, *108*, 10625.
(12) Ivanov, S. A.; Piryatinski, A.; Nanda, J.; Tretiak, S.; Zavadil, K. R.; Wallace, W. O.; Werder, D.; Klimov, V. I. *J. Am. Chem. Soc.* **2007**, *129*, 11708.
(13) Pandey, A.; Guyot-Sionnest, P. *J. Phys. Chem. B* **2007**, *127*, 104710.
(14) Reiss, P.; Protiere, M.; Li, L. *Small* **2009**, *5*, 154.
(15) Carbone, L.; Nobile, C.; De Giorgi, M.; Della Sala, F.; Morello, G.; Pompa, P.; Hytch, M.; Snoeck, E.; Fiore, A.; Franchini, I. R..; et al. *Nano Lett.* **2007**, *7*, 2942.
(16) Dorfs, D.; Salant, A.; Popov, I.; Banin, U. *Small* **2008**, *4*, 1319.
(17) Hewa-Kasakarage, N. N.; Kirsanova, M.; Nemchinov, A.; Schmall, N.; El-Khoury, P. Z.; Tarnovsky, A. N.; Zamkov, M. *J. Am. Chem. Soc.* **2009**, *131*, 1328.
(18) Shieh, F.; Saunders, A. E.; Korgel, B. A. *J. Phys. Chem. B* **2005**, *119*, 8539.
(19) Halpert, J. E.; Porter, V. J.; Zimmer, J. P.; Bawendi, M. G. *J. Am. Chem. Soc.* **2006**, *128*, 12590.
(20) Shi, W.; Zeng, H.; Sahoo, Y.; Ohulchanskyy, T. Y.; Ding, Y.; Wang, Z. L.; Prasad, P. N. *Nano Lett.* **2006**, *6*, 875.
(21) Heng, Y.; Chen, M.; Rice, P. M.; Wang, S. X.; White, R. L.; Sun, S. *Nano Lett.* **2005**, *5*, 379.
(22) Carbone, L.; Kudera, S.; Carlino, E.; Parak, W. J.; Giannini, C.; Cingolani, R.; Manna, L. *J. Am. Chem. Soc.* **2006**, *128*, 748.
(23) Milliron, D. J.; Hughes, S. M.; Cui, Y.; Manna, L.; Li, J.; Wang, L.; Alivisatos, A. P. *Nature* **2004**, *430*, 190.
(24) Kumar, S.; Jones, M.; Lo, S. S.; Scholes, G. D. *Small* **2007**, *3*, 1633.
(25) Fiore, A.; Mastria, R.; Lupo, M. G.; Lanzani, G.; Giannini, C.; Carlino, E.; Morello, G.; Giorgi, M. D.; Li, Y.; Cingolani, R.; Manna, L. *J. Am. Chem. Soc.* **2009**, *131*, 2274.

Published on Web 08/14/2009

well as accessibility of separated charges for a redox reaction in photovoltaic devices were realized using a barbell architecture, formed by capping CdSe nanorods with CdTe NCs on either one or both sides. These heterostructured barbells have been extensively investigated toward improving the quality of the CdTe/CdSe interface,[26,27] where an intrinsic lattice strain (lattice mismatch $\approx 6\%$) results in the formation of interfacial defects and the interdiffusion of Te and Se ions, which creates carrier trapping sites and leads to the suppression of room-temperature luminescence.

Here, we report on a colloidal synthesis of type II nanobarbells comprising a nearly lattice-matched ZnSe/CdS/ZnSe combination of materials (mismatch $\sim 2.7\%$) and showing an improved interfacial crystallinity, as was evidenced by the observation of "spatially indirect" fluorescence (FL) at room temperature. An anisotropic growth of ZnSe caps onto CdS NRs was possible due to an intrinsically higher rate of Zn and Se monomer addition in [000 $\pm$ 1] crystallographic directions of wurtzite CdS NRs, which helped in suppressing the lateral growth of the ZnSe shell to a fraction of a monolayer. As a result, both CdS and ZnSe material domains of fabricated ZnSe/CdS nanobarbells are exposed to the NC surroundings, providing direct pathways for a transfer of separated electrons and holes to redox agents, if proper organic ligands are chosen. Such accessibility of photoinduced carriers for an external reaction was not allowed in a previously developed dot-in-a-rod or tetrapod ZnSe/CdS architectures, where the photoexcited hole remains trapped inside the ZnSe core due to a passivating layer of CdS material. In addition, the use of ZnSe/CdS semiconductor combination in lieu of CdTe/CdSe materials in a barbell arrangement should lead to the increased spatial separation of excited carriers along the main barbell axis, as can be expected from a greater offset of band edges at the junction of ZnSe and CdS domains (see ref 28).

2. Experimental Section

2.1. Chemicals. Sulfur (99.999%, Acros), 1-octadecene (ODE, tech., 90%, Aldrich), cadmium oxide (99.99%, Alrdich), oleic acid (OA, tech., 90%, Aldrich), tri-*n*-octylphosphine (TOP, 97%, Strem), tri-*n*-octylphosphine oxide (TOPO, 99%, Aldrich), *n*-octadecylphosphonic acid (ODPA, PCI Synthesis), *n*-hexylphosphonic acid (HPA, PCI Synthesis), octadecylamine (ODA, 90%, tech., Acros), zinc oxide (99+%, Aldrich), selenium (99.5+%, Acros), hexane (anhydrous, 95%, Aldrich), methanol (99.8+%, EMD), toluene (anhydrous, 99.8%, Aldrich), and chloroform (anhydrous, 99+%, Aldrich) were used. All chemicals were used as received without any further purification. All reactions were performed under argon atmosphere using the standard Schlenk technique.

CdS nanorods were synthesized using a seeded-type approach by introducing small-diameter CdS nanocrystals into the reaction mixture for nucleating the growth of linear CdS extensions, according to the procedure adapted from ref 15. The original CdS seeds were not distinguishable in fabricated CdS nanorods.

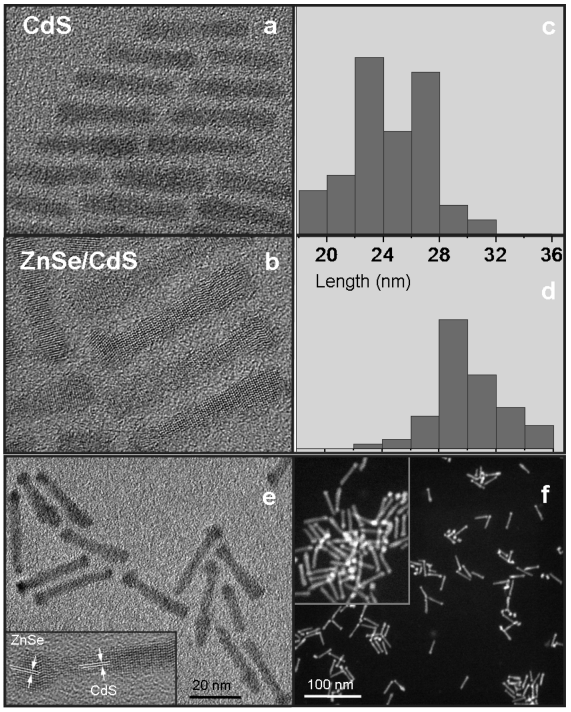

Figure 1. High-resolution TEM images showing CdS nanorods (a) and ZnSe/CdS nanobarbells (b), along with the corresponding statistical distributions of lengths in (c) and (d), respectively. TEM (e) and HAADF-STEM (f) images of ZnSe/CdS nanobarbells.

2.2. Synthesis of CdS Nanocrystals. CdS seeds were fabricated according to the procedure reported in ref 29. In a typical synthesis, the mixture of cadmium oxide (0.0384 g), OA (0.9 mL), and ODE (12.0 mL) in a 50 mL 3-neck flask was heated to 300 °C until the solution turned optically clear and colorless. At this point, a sulfur precursor solution made by dissolving sulfur powder (0.0048 g) in ODE (4.5 mL) at 200 °C was quickly injected, and the temperature was stabilized at 260 °C for the nanocrystal growth. The reaction was stopped after 5−9 min, and nanocrystals were isolated from the growth solution by precipitation with methanol, followed by repeated hexane/methanol extractions. The average diameter of fabricated CdS nanocrystals was in the range of 3.5−4.0 nm, depending on the growth time.

2.3. Synthesis of CdS Nanorods. The amount of CdS seeds for the synthesis of CdS nanorods was calculated using an empirical approach, whereby the product of the particle absorption at 400 nm (excitonic feature) and the volume of the colloidal suspension (in mL) was set to be in the range of 5−10. For instance, CdS nanorods shown in Figure 1a were synthesized using 8 units of CdS seeds. Overall, it was determined that using lower amounts of CdS seeds generally yields high-aspect ratio nanorods, however, when less than 5 units of CdS is used for seeding, a small amount of tetrapods can also form during the reaction, alongside high-aspect-ratio nanorods. In a typical synthesis of CdS nanorods, CdS seed powder was dispersed in 1.8 mL of TOP and subsequently introduced (at 60 °C) into the sulfur injection solution, previously prepared by dissolving sulfur (0.120 g) in TOP (1.81 mL) at 200 °C. Separately, the mixture of cadmium oxide (0.060 g), TOPO (3.0 g), ODPA (0.290), and HPA (0.080 g) in a 50 mL 3-neck flask was exposed

(26) Saunders, A. E.; Koo, B.; Wang, X.; Shih, C. K.; Korgel, B. A. *ChemPhysChem* **2008**, *9*, 1158.
(27) Koo, B.; Korgel, B. A. *Nano Lett.* **2008**, *8*, 2490.
(28) Nemchinov, A.; Kirsanova, M.; Hewa-Kasakarage, N. N.; Zamkov, M. *J. Phys. Chem. C* **2008**, *112*, 9301.
(29) Yu, W. W.; Peng, X. *Angew. Chem.* **2002**, *114*, 2474.

to vacuum at 150 °C for ca. 30 min. Subsequently, the system was switched to Ar flow and heated to above 350 °C until the solution turned optically clear and colorless. At this point, TOP (1.81 mL) was added to the flask as the Cd precursor coordinating solvent. The rod growth was initiated by a quick injection of the seed/sulfur solution at 380 °C. After the temperature recovered to 350 °C the nanorods were allowed to grow for an additional 7−9 min. Purification of CdS nanorods was similar to those of CdS seeds.

2.4. Synthesis of ZnSe/CdS Nanobarbells. In a typical procedure, 0.5 mL of hexane-suspended CdS nanorods (60 times diluted injection volume showed the excitonic absorption peak of 0.75, which corresponds to approximately 12 mg of dry nanorods) was injected into a degassed mixture of ODE (6.0 mL) and ODA (1.5 g) at 80 °C and pumped for about 20 min to remove hexane and any residual air from the system. At this step, the system was switched to Ar flow and heated to 250 °C before injecting the precursors. Zinc injection solution was prepared by heating zinc oxide (0.0350 g), OA (1.2 mL), and TOP (1.5 mL) to above 250 °C until the solution was clear. Subsequently, it was allowed to cool to about 60 °C and mixed with the Se:TOP precursor (0.0340 g of selenium and 0.7 mL of TOP). During the nanobarbell growth the precursor solution was added via syringe to the reaction flask kept at 245 °C in 0.1 mL amounts every 2 min. After 10−20 min, the reaction was stopped by cooling the flask to approximately 50 °C and adding excess toluene.

2.5. Purification of CdS/CdS/ZnSe Nanobarbells. The final product was precipitated from toluene by adding methanol and chloroform (3:1) at 50 °C. The subsequent cleaning was done using hexane/methanol extraction where a minimal amount of chloroform was introduced for mixing of hexane and methanol layers.

2.6. Characterization. UV−vis absorption and photoluminescence spectra were recorded using CARY 50 Scan spectrophotometer and Jobin Yvon Fluorolog FL3-11 fluorescence spectrophotometer. FL quantum yield (QY) was determined relative to known QYs of several organic dyes excited at 400−440 nm. High resolution transmission electron microscopy measurements were carried out using JEOL 3011UHR operated at 300 kV. High angular annular dark field scanning transmission electron microscopy was performed using JEOL 2010 transmission electron microscope. Specimens were prepared by depositing a drop of nanocrystal hexane solution onto a Formvar-coated copper grid and letting it dry in air. X-ray powder diffraction measurements were carried out on Scintag XDS-2000 X-ray powder diffractometer. Energy dispersive X-ray (EDX) emission spectra were measured using an EDAX X-ray detector located inside a scanning electron microscope. The electron beam was accelerated at 20 kV.

2.7. Fluorescence Lifetime Measurements. FL lifetime measurements (Figure 3) were performed using a time correlated single photon counting setup utilizing SPC-630 single photon counting PCI card (Becker & Hickle CmbH), picosecond diode laser operating at 400 nm, as an excitation source (Picoquant), and id50 avalanche photodiode (Quantique). The repletion rate of the laser was chosen to allow for a 1000 ns time window while the pulse fluence was adjusted to produce about 1 emission photon per 100 excitation pulses.

3. Results and Discussion

Growth of ZnSe caps onto previously prepared CdS NRs was performed in a mixture of octadecene (ODE) and trioctylphosphine (TOP) solvents using ZnO/oleic acid (OA) combination as a precursor of zinc. Initial efforts to use zinc stearate in octadecane or $ZnEt_2$ in TOP did not result in a rapid monomer addition, which was needed to avoid thermal coalescing of CdS NRs.[30] Interestingly, a heterogeneous growth of ZnSe along [000 ± 1] directions was achieved without the use of hexylphosphonic acid (HPA), which was routinely employed in the synthesis of CdSe and CdTe NRs for suppressing the growth along 100 and 110 crystalline axes.[31] In the absence of site-selective ligands, the preferential attachment of ZnSe onto polar facets of CdS NRs is attributed to the higher-energy threshold for the homogeneous (lateral) expansion, which is consistent with the growth regime characterized by a low monomer concentration.[17]

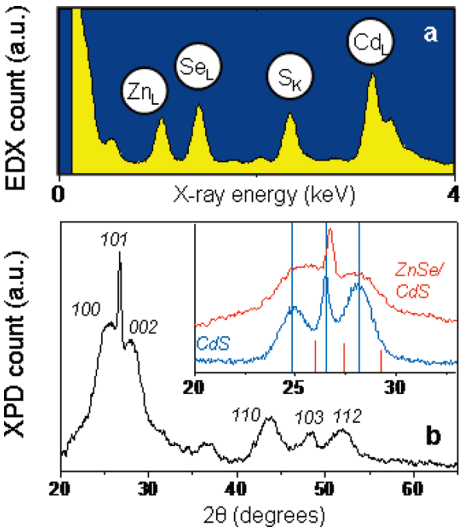

Figure 2. EDX (a) and XPD (b) spectra of ZnSe/CdS nanobarbells confirming the presence of both CdS and ZnSe nanocrystal domains.

Transmission electron microscopy (TEM) analysis of grown heterostructures (Figure 1b) shows an average 5.2-nm elongation along the wurtzite *c*-axis in comparison with starting CdS NRs (Figure 1a), as well as an apparent formation of either one or two-sided ZnSe caps, whose unique elemental composition was evident through the color contrast in high angular annular dark field scanning transmission electron microscopy (HAADF-STEM) (Figure 1f). According to statistical size histograms in Figures 1c,d, growth of ZnSe sections is accompanied by a moderate focusing of the total length distribution, corresponding to the decrease of the standard deviation from 11% (nanorods) to 8.1% (nanobarbells). The average barbell width was found to increase during synthesis from 3.98 to 4.12 nm, which is equivalent to the addition of 0.2 monolayers of ZnSe on a side wall of CdS NRs. This result is consistent with the energy dispersive X-ray (EDX) analysis of the barbell elemental composition (Figure 2a) showing a somewhat greater-than-expected amount of Zn and Se in fabricated heterostructures. Overall, fairly good

(30) Puntes, V. F.; Krishnan, K. M.; Alivisatos, A. P. *Science*. **2001**, *291*, 2115.
(31) Manna, L.; Scher, E. C.; Alivisatos, A. P. *J. Am. Chem. Soc*. **2000**, *122*, 12700.

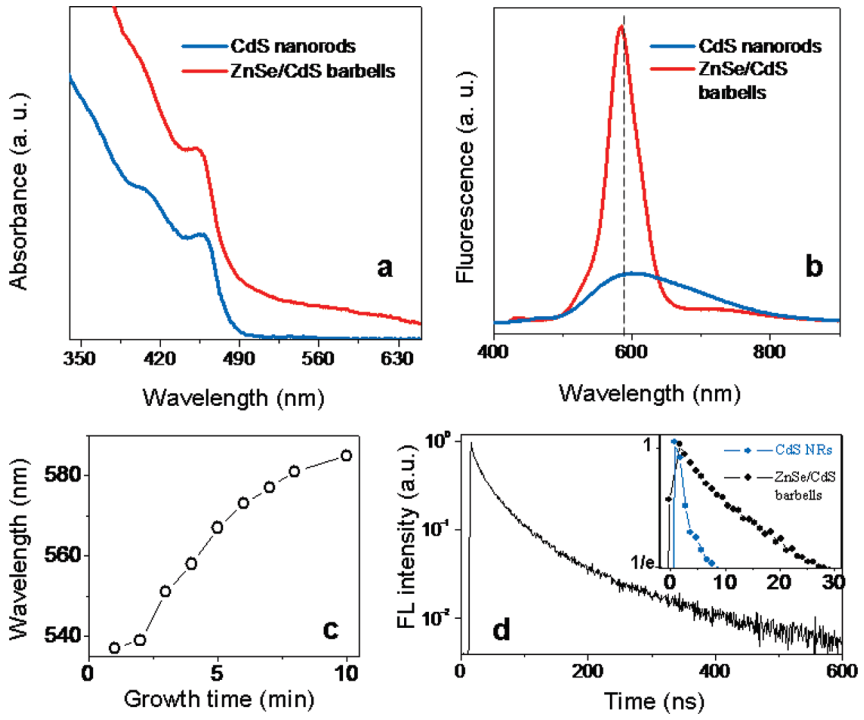

Figure 3. Absorption (a) and emission (b) spectra of CdS nanorods (blue) and ZnSe/CdS nanobarbells (red). (c) Spectral evolution of the emission peak during deposition of ZnSe. (d) FL intensity decay of charge-transfer states.

monodispersity of nanobarbells' lengths (8.1%) and widths (8.9%) was observed.

X-ray powder diffraction (XPD) measurements (Figure 2b) confirmed the wurtzite structure of the ZnSe/CdS heterocrystal lattice. As expected, the deposition of ZnSe caps causes characteristic Bragg peaks to shift toward higher angles with respect to those in CdS NRs due to smaller lattice spacing of the ZnSe phase. The two separate sets of peaks corresponding to CdS and ZnSe bulk phases, however, cannot be distinguished. Instead the observed pattern is characterized by a rather homogeneous broadening of diffraction features, which is consistent with the presence of a lattice stress in the overgrown ZnSe material, particularly in the surface and interfacial areas, as was previously observed for CdS/ZnSe core/shell NCs.[32] As a result of a relatively small lattice mismatch, such lattice strain, however, does not prevent interfacial charge transfer, as evident by the spectrally narrow emission peak (Figure 3b) arising from the recombination of separated carriers. In addition, the large surface area-to-volume ratio, characteristic to small-diameter nanobarbells, further relieves strains at the epitaxial interface of ZnSe and CdS, thus alleviating the formation of extended defects.[33]

Absorption spectra of fabricated nanobarbells (Figure 3a) are typical of type II heterostructures with nonzero photon absorption in the spectral range below the band gap of both ZnSe and CdS NCs. This is expected due to excitations of intermediate states that exist at the junction of both materials, as evident by the onset of the 500−600 nm tail. Similar kinetics of spectral changes was previously reported for CdSe/CdTe nanobarbells, where the absorption range was found to extend below the band gap of both CdSe and CdTe NCs. In contrast to CdSe/CdTe heterostructures, however, ZnSe/CdS nanobarbells exhibit room-temperature FL that matches the recombination energy of charge transfer states, $1S_e$(CdS)-$1S_h$-(ZnSe), as shown in Figure 3b. Indeed, upon deposition of ZnSe material, the broad emission of trap states in CdS NRs is partly quenched, giving rise to a narrow emission feature, whose spectral evolution reflects the expected[21,28] decrease in the carrier confinement associated with the onset of type II localization regime (Figure 3c). The quantum yield of emission was in the range of 4−6%.

The dynamics of carrier decay in ZnSe/CdS nanobarbells was further investigated using FL lifetime measurements (Figure 3d). The observed relaxation time of 28 ns exceeds the lifetime of the trap state emission in CdS NRs by a factor of 4, which is consistent with a decreased overlap of delocalized electron and hole wave functions in ZnSe/CdS nanobarbells. The measured lifetime, however, is strongly affected by the hole trapping on the surface of ZnSe NCs, which was consistent with the observation of a considerable solvent effect on the measured FL lifetime (±30%, for toluene, hexane, and chloroform). Indeed, compared to dot-in-a-rod heterostructures, where photoinduced holes are passivated by a thick layer of CdS material, the architecture of ZnSe/CdS nanobarbells exposes both charges to surface traps and therefore induces carrier interactions with the caging media. Similarly photoexcited electrons can also participate in external interaction: the submonolayer (0.2 ML)

(32) Ivanov, S. A.; Piryatinski, A.; Nanda, J.; Tretiak, S.; Zavadil, K. R.; Wallace, W. O.; Werder, D.; Klimov, V. I. *J. Am. Chem. Soc.* **2007**, *129*, 11708.
(33) Chen, X. B.; Lou, Y. B.; Samia, A. C.; Burda, C. *Nano Lett.* **2003**, *3*, 799.

ZnSe shell that partly covers the surface of a CdS domain is too thin to create a potential barrier that would confine electrons within nanorods or to prevent electron trapping at the surface. As a result, the effect of lifetime dilation, which is expected for spatially separated carriers due to weaker confinement, is not as pronounced for ZnSe/CdS nanobarbells, as in the case of ZnSe/CdS nanorods.

In summary, we have demonstrated solution-phase synthesis of heterostructured nanobarbells comprising a staggered heterojunction of nearly lattice-matched ZnSe and CdS semiconductors and showing compelling evidence of photoinduced charge separation. Fabricated nanomaterials benefit from the assimilation of ZnSe/CdS heterojunction within a barbell architecture, which allows combining a large type II offset of band edges with the availability of photogenerated holes for external reactions. Such a combination of properties can be harnessed in diverse realizations of photoinduced charge separation in colloidal nanoparticles, including photovoltaic and photocatalytic technologies.

Acknowledgment. We gratefully acknowledge Bowling Green State University for financial support (SF07, RIC2008, RCE2008).

Supporting Information Available: Full author list for ref 15 and Figure S1 (PDF). This material is available free of charge via the Internet at http://pubs.acs.org.